

A Discrete Vortex Method for Simulating a Stand-Alone Tidal-Current Turbine: Modeling and Validation

Ye Li¹
e-mail: ye.li@nrel.gov

Sander M. Çalıřal

Department of Mechanical Engineering,
University of British Columbia,
6250 Applied Sciences Ln,
Vancouver, BC, V6T1Z4, Canada

This paper advanced our recent effort (Li and Çalıřal, 2007, "Preliminary Result of a Discrete Vortex Method for Individual Marine Current Turbine," The 26th ASME International Conference on Offshore Mechanics and Arctic Engineering, Jun. 10–15, San Diego, CA) to study the behavior of tidal-current turbines. We propose a discrete-vortex method with free-wake structure (DVM-UBC) to describe the behavior of a stand-alone tidal-current turbine and its surrounding unsteady flow and develop a numerical model to predict the performance and wake structure of the turbine based on DVM-UBC. To validate this method, we conducted a series of towing tank tests. DVM-UBC is then validated with several kinematic and dynamic results. When we compared the results obtained with DVM-UBC with our towing tank test results, published results, and the results obtained with other numerical methods, we achieved good agreements. Our comparisons also suggested that DVM-UBC can predict the performance of a turbine 50% more accurately than the traditional discrete-vortex method (traditional DVM) with comparable computational effort and will produce results comparable to the Reynolds averaged Navier–Stokes equation with much less computational effort.
[DOI: 10.1115/1.4000499]

Keywords: tidal power, tidal-current, discrete-vortex method, unsteady flow, viscous effect, numerical simulation, kinematic and dynamic validation, towing tank test

1 Introduction

This paper describes our use of a discrete-vortex method with free-wake structure (DVM-UBC)² for simulating tidal-current turbines and is an extension of the work we presented in OMAE 2007 [1]. Tidal-current as an energy resource has the advantages of being renewable and predictable, and tidal-current turbines have low visual and environmental impacts compared with other alternative energy conversion technologies [2]. Tidal-current turbines extract energy from tidal currents and are similar in principle to wind turbines. Tidal-current turbines are classified as either horizontal-axis or vertical-axis turbines. A horizontal-axis tidal-current turbine's shaft is located on a horizontal plane, and a vertical-axis tidal-current turbine's shaft is located on a vertical plane. In this paper, we focus on vertical-axis tidal-current turbines.

Unlike the wind power industry, which is quite mature, the tidal-current power industry is still in its infancy. There is still substantial research to be done before tidal-current turbines can be commercialized. The numerical and experimental investigation of tidal-current turbines was started in the 1980s by the Canadian National Research Council (NRC) [3–5]. The experimental tests at NRC were conducted in a restricted water flume, and the results cannot be extrapolated to represent the behavior of a turbine in open waters. The numerical method employed by the NRC was the simplest potential-flow method (i.e., the momentum method). Thereafter, only a handful of experimental and numerical investigations on tidal-current turbines were carried out. Because these

laboratory tests were constrained by a lack of funding, they were conducted either in a water flume or in a narrow tank [6,7]. The numerical methods developed are either computationally costly or fail to accurately simulate the behavior and performance of tidal-current turbines in the highly unsteady flow of open water.

The existing numerical methods can be sorted as Reynolds averaged Navier–Stokes (RANS) equation methods and potential-flow methods. RANS methods can predict the performance of turbines with high accuracy if the meshes are fine enough, but the associated computational cost is extremely high [8,9]. Regarding the potential-flow methods, the momentum method [10,11] and the boundary-element method [7] are used to predict power output from a turbine; the blade element method [6] is used to predict the force on the blade of a turbine; the finite element method [12] is used to predict the wake of a turbine; the boundary-element method coupled with the finite element method [13] is used to predict the surface pressure on the blade of a turbine; and the vortex method [1], which we develop and extend in this paper, is used to predict the power output and the wake of a turbine. Of all the methods described above, only the vortex method and the boundary-element method predict all important characteristics (e.g., power output, torque, and wake) of tidal-current turbines [14]. Comparatively, the vortex method is more suitable for simulating a turbine to fully understand the rotation of the turbine and the unsteady wake, and the boundary-element method can provide a more detailed description of force and pressure on the blade surface. Particularly, DVM-UBC has the advantages of being able to describe the unsteady nature of wake structure (compared with momentum method and vortex method with fixed wake structure, e.g., Refs. [15,16]), and being computationally inexpensive (compared with commercial RANS packages).

To verify that DVM-UBC can simulate the physics of the flow and the turbine's operation accurately, we conducted experiments in the towing tank at the University of British Columbia (UBC) and compared the results obtained with DVM-UBC with the ex-

¹Present address: National Wind Technology Center, National Renewable Energy Laboratory, 1617 Cole Blvd., MS 3811, Golden, CO 80401.

²This method is a discrete-vortex method. We call it as DVM-UBC because it was developed by the researchers in the University of British Columbia (UBC).

Contributed by the Ocean Offshore and Arctic Engineering Division of ASME for publication in the JOURNAL OF OFFSHORE MECHANICS AND ARCTIC ENGINEERING. Manuscript received December 1, 2008; final manuscript received September 15, 2009; published online April 7, 2010. Assoc. Editor: Sergio Sphaier.

perimental results. We also compared the DVM-UBC results with other published experimental results, as well as the results obtained with other numerical methods (e.g., traditional discrete-vortex method and RANS). Compared with the validation used for previous potential-flow methods, which were validated with either one dynamical result or one kinematic result, our validation is comprehensive because we compare a series of both the dynamic and kinematic results.

Overall, the purpose of this study is to develop a cost-effective numerical method to simulate the behavior of a stand-alone turbine and the unsteady flow. For this purpose, we formulated DVM-UBC, as detailed in Sec. 2. Section 3 describes the experimental tests we conducted in the UBC towing tank to validate the DVM-UBC. Section 4 describes the validation process. We discuss the results, especially our findings obtained with the UBC towing tank tests, and our conclusions in Sec. 5.

2 Modeling

We developed a cost-effective numerical method for approximating the rotation of a tidal-current turbine and the unsteady flow surrounding the turbine, i.e., DVM-UBC, based on the traditional discrete-vortex method (DVM). In this section, we recapitulate the formulation of the traditional DVM, then present a detailed description of the DVM-UBC about the flow and the turbine. The final calculation of force and torques of the turbine is not related to the formulation of vortex method so that it is given in the Appendix. To formulate a rigorous mathematical model to describe the hydrodynamics of a tidal-current turbine and the unsteady flow, we made the following assumptions.

- The tidal-current turbine works as a stand-alone turbine. There are no auxiliary structures (such as ducts and anchors) and other turbines around the studied turbine.
- The incoming flow is uniform.
- Each blade of the turbine is divided into several finite segments (elements) along the span of the blade with a given geometry, and each blade element is represented by a bound vortex.
- The lift and drag on a blade element are calculated by using steady-state lift and drag coefficients that are obtained with experiments.
- In the wake of the blade, the production, convection, and interaction of the vortex system shed from individual blade elements are modeled based on the induced velocity concept. The phenomenon of vortex shedding obeys Kelvin's theorem (see Eq. (1)).

$$\frac{D\Gamma}{Dt} = 0 \quad (1)$$

where Γ and t denote the circulation and time, respectively.

- In the wake, the velocity at a single point can be simplified by superimposing all the induced velocities upon the undisturbed incoming flow velocity.
- The effects from the shaft, supporting arm, and blade controller on the performance of the turbine are obtained from experiments. Shaft and shaft-induced wake structure are not considered in this formulation.

2.1 Basic Formulation. When the vortex method is used for simulating the flow around a turbine, the velocity of the local fluid (e.g., at point p), U_V , is the vectorial sum of the incoming flow velocity, U_∞ , and the aggregated induced velocity, U_{iP} , given as

$$U_V = U_\infty + U_{iP} \quad (2)$$

The aggregated induced velocity is the sum of the velocities induced by all vortices in the computational domain. According to the Biot–Savart law [17], given a vortex filament of an arbitrary shape with a strength of Γ and a length of l (e.g., a turbine blade

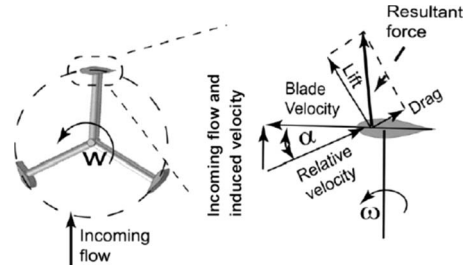


Fig. 1 An illustration of turbine working principle. (This illustration does not represent the configuration and the scale of a real turbine. Also, induced velocity is not depicted due to the uncertainty of its direction.)

element), the induced velocity at point p (but not on the filament) can be calculated as

$$U_{iP,l} = \frac{\Gamma}{4\pi} \int_l \frac{\mathbf{r} \times d\mathbf{l}}{r^3} \quad (3)$$

where \mathbf{r} denotes the position vector from a point on the filament to point p .

The vortices filaments here includes both blade bound vortex and wake vortex. The strengths of these vortices depend on the operation of the turbine. To model the turbine's operation, we need to understand the turbine's working principle. Figure 1 depicts a working turbine and one zoomed-in blade element (cross section). The turbine rotates at a certain angular velocity, ω , driven by the force of the incoming flow on the blades. At this angular velocity, the tip velocity of the turbine blade, U_t , can be written as

$$U_t = R\omega \quad (4)$$

where R denotes the radius of the turbine.

The incoming flow and the turbine's rotation introduce an angle of attack, α , which is the angle between the local relative velocity seen by the blade and the blade chord line. The angle of attack can be obtained by resolving the relative velocity seen by the blade, U_R , and the chord line of the blade according to their vectorial relationship, as shown in Fig. 1. One can calculate the angle of attack with respect to the nose of the foil or at 1/4 chord length from the nose of the blade. In this paper, we calculate it at 1/4 chord length from the nose of the blade. The relative velocity seen by the blade is the flow velocity seen by the blade element, which is a function of the free stream incoming velocity, U_∞ , the induced velocity at the blade, U_{iB} , and the tip velocity of the blade, U_t . Mathematically, it can be written as

$$U_R = U_\infty + U_{iB} + U_t \quad (5)$$

The lift and drag generated by the incoming flow are directly related to this angle of attack. The resultant force on a blade element can be calculated by summing the lift and the drag. The relationship between lift, L , and bound vortex strength, Γ_B , on a blade segment is employed to derive the relationship between blade bound vortex strength and shedding vortex strength. The former relationship can be derived by using the Kutta–Joukowski law [17] as

$$L = \rho U_R \Gamma_B \quad (6)$$

where ρ denotes the density of sea water.

According to the definition of lift coefficient, the lift can be obtained by using Eq. (7)

$$L = \frac{1}{2} \rho C_L c U_R^2 \quad (7)$$

where C_L and c denotes the lift coefficient and the chord length,

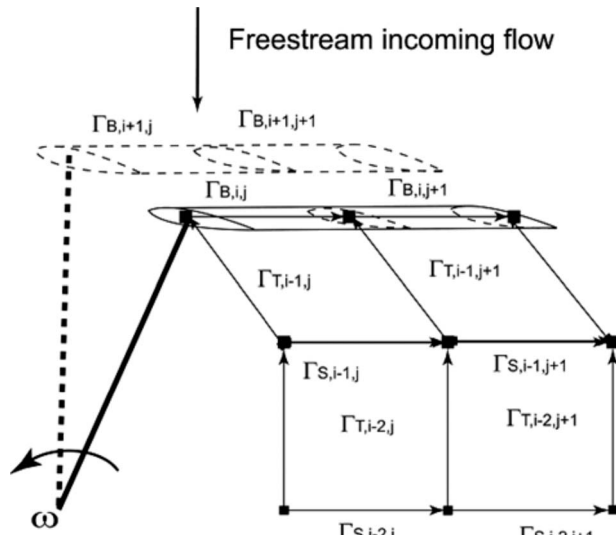


Fig. 2 An illustration of a three-dimensional time-dependent vortex wake structure

respectively.

By combining Eqs. (6) and (7), we can express the strength of the bound vortex as

$$\Gamma_B = \frac{1}{2} C_L C U_R \quad (8)$$

Figure 2 shows the structure of a three-dimensional wake vortex system of a blade with two elements. This vortex system is initially assumed to be of horseshoe shape. The spanwise vortex filament strength, Γ_S , and the trailing edge vortex filament strength, Γ_T , can be written as

$$\Gamma_{S,i-1,j} = \Gamma_{B,i-1,j} - \Gamma_{B,i,j} \quad (9)$$

$$\Gamma_{T,i-1,j} = \Gamma_{B,i,j} - \Gamma_{B,i,j-1} \quad (10)$$

where i is the index of the time step and j is the index of the blade element.

So numerically, by summing velocities induced by all vortex filaments using Eq. (3), the aggregated induced velocity at any given point p can be written as

$$U_{iP} = \sum_i \sum_j V_{iPT,i,j} + \sum_i \sum_j V_{iPS,i,j} \quad (11)$$

where $V_{PT,i,j}$ denotes the velocity induced by the trailing edge wake vortices shed from blade element i at time step j , and $V_{PS,i,j}$ denotes the velocity induced by the spanwise wake vortices shed from the same element.

2.2 Introducing Viscous Effects. The mathematical description of the traditional DVM (mentioned above) neglects the nascent vortex and does not allow viscous diffusion that can induce decay of vortices. Although this simplification reduces the computational cost and is acceptable for wind turbine application, it is not acceptable for marine applications because of the viscous effects. To get a better approximation to the unsteady flow and to achieve more stable computational results, in this study we simulate the nascent vortex and allow the vortices to decay with time in the wake by introducing several artificial terms.

For the nascent vortex, we must avoid the singularity issues near the blade. Streitlien [18] found that the nascent vortex starts at a certain point determined by interpolating the trailing edge and the last vortices depending on the motion of the blade. Considering the high shedding frequency, we suggest that the location of the nascent vortex be set in the middle point between the trailing

edge and the last vortex. That is, if the location of the trailing edge of a blade at time t_o is (x_{t_o}, y_{t_o}) , the location of the nascent vortex (vortex m) can be given as

$$x_{V,m}|_{t=t_o} = \frac{1}{2}(x_{t_o} + x_{V,m-1}|_{t=t_o}) \quad (12)$$

$$y_{V,m}|_{t=t_o} = \frac{1}{2}(y_{t_o} + y_{V,m-1}|_{t=t_o})$$

Accordingly, we suggest that the nascent vortex velocity be half of the last vortex velocity (vortex $m-1$). That is, at time t_o , the velocity of the nascent vortex is

$$U_{V,m}|_{t=t_o} = \frac{1}{2} U_{V,m-1}|_{t=t_o} \quad (13)$$

where $U_{V,m}|_{t=t_o}$ denotes the velocity of vortex m at time t_o . At the same time, the velocity of last vortex can be obtained by substituting the nascent vortex definition into Eq. (11) as

$$U_{V,m-1}|_{t=t_o} = U_\infty + U_{iP,m-1} \quad (14)$$

At the next time step, vortex m is no longer a nascent vortex, and its velocity is written as

$$U_{V,m}|_{t=t_o+\Delta t} = U_\infty + U_{iP,m} \quad (15)$$

Vortex shedding frequency can either be obtained by experimental testing or it can be estimated using the Strouhal number, St , as given in Eq. (12), together with the Reynolds number, which has been recently successfully used in the investigation of ocean energy conversion devices by Bernitsas et al. [19] and is given as

$$f = \frac{St U_R}{c} \quad (16)$$

where St denotes the Strouhal number.

To get a better approximation to the unsteady flow in the wake and achieve more stable computational results, vortices are allowed to decay with time, as suggested by Graham [20], and written as

$$\Gamma_j = \Gamma_0(1 - e^{(-K_d t/\tau)}) \quad (17)$$

where K_d denote vortex strength decay coefficient, which can be obtained from experiments or predicted using numerical methods for a body of a specific shape.

In DVM-UBC, the unsteady flow is represented by a large group of vortices and a uniform flow. In the calculation, the number of vortices increases as the turbine rotates. A large number of vortices require a large memory space in the computer. This significantly increases the computational cost. The vortex strength decays exponentially with distance or time, and it almost vanishes beyond a certain range. Kudo [21] successfully set a critical distance to enforce the vortex die out when vortex decay is evaluated for a study of flat plate. When vortex shedding from a tidal-current turbine is calculated, given the vortex decay is significantly influenced by the turbine rotation, a critical number of turbine revolutions, i.e., critical time is set to substitute the critical distance, which means that the vortex vanishes after a number of turbine revolutions after it is shed. Here, the critical number of turbine revolutions is set to ten.

3 Experimental Setup in UBC-Towing Tank

In parallel with the numerical investigation, a series of tidal-current turbines with different blade profiles and geometries were designed, built, and tested in the towing tank at UBC. This experiment was based on the optimization recommendations from the numerical investigation. The purpose of the experimental test was to produce a more accurate simulation of a turbine in a free stream than previous tests produced. For example, the turbine tested by Strickland [22] was only partially submerged, and free-surface effects were induced. In this case, the free-surface affected wave loads on the blades so that the measured force and torque deviated from the force and torque found on a fully submerged



Fig. 3 An illustration of one of the turbines designed at UBC with the mounting frame

turbine in the ocean. In another example, the experimental tests reported by Davis et al. [3] were conducted in a confined water flume where the turbine almost entirely blocked the flume. In this case, the wall of the channel is very close to the turbine, and the blockage effect increased the incoming flow velocity. As a result, the power output of the turbine is significantly higher than that of a turbine in free stream. Additionally, some experimental results are used to validate the numerical model.

The experimental models used for validation in this paper are a 0.9 m diameter three-blade vertical-axis turbine and a 0.91 m diameter single-blade vertical-axis turbine. The foil section used for the blades is an NACA 63₍₄₎-021 section with an ideal chord length of 0.0686 m, of which the trailing edge is cropped to 0.065 m to facilitate the manufacture. The blades are mounted to the central shaft of the turbine by two arms connected at the quarter-span locations. The arms are fixed to the blades using a pivot joint with a clamping mechanism such that the angle of attack can be adjusted using precision-wedges.

Figure 3 shows how an individual turbine is installed on a mounting frame and fully submerged in the water during the test. Both the turbine and the mounting frame are made of aluminum. The lower shaft bearing is supported by a U-shape frame. The upper shaft bearing is mounted above the water surface onto a force balance consisting of two parallel plates capable of translating forces relative to each other and connected via load cells. The load cells are used to measure the drag force exerted on the turbine as it is towed through the water. The turbine revolution speed is controlled using an ac motor controller. An optical encoder is used to measure rotational speed and angular position of the main shaft. A torque meter is connected inline to measure the torque produced by the turbine.

The UBC towing tank is 67 m long, 3.7 m wide, and 2.4 m deep, which is large enough to significantly reduce the wall effects

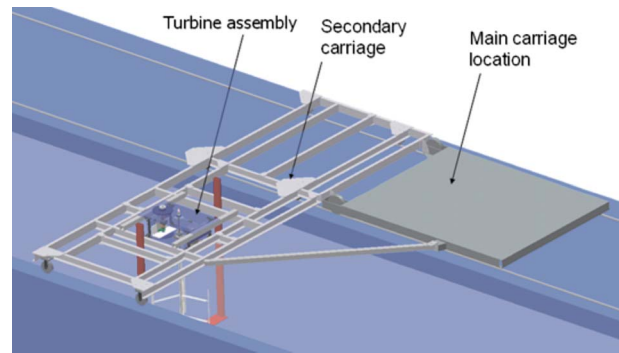


Fig. 4 Testing facility of UBC towing tank

and free-surface effects in the previous tests conducted by Davis et al. [3] and Strickland [22]. The UBC towing tank was designed and built for testing ship models in the late 1970s. The main carriage (a ship testing carriage), which runs on the rails along the side of the tank, is not capable of supporting the turbine mounting frame. Thus, a secondary carriage was designed and attached to the main carriage with a diagonal brace to provide additional support, as shown in Fig. 4. This secondary carriage is made of welded aluminum c-channel in two halves that are bolted together. Two v-grooved wheels run along the inner rails that are closer to the tank, and two rubber wheels rest on the outer rails that are farther from the tank. The maximum speed of the carriage during the test is 2 m/s and the turbine's tip speed ratio (TSR) varies from 1.25 to 3.5.

In this paper, the results from the UBC towing tank experimental test are used for the purpose of hydrodynamic analysis and validation. Therefore, we do not provide detailed information on electronic devices. Readers who are interested in the setup of electronic devices and data acquisition techniques can refer to Ref. [23].

4 Validation

To develop and conduct a comprehensive validation, we validate the results obtained with DVM-UBC in both dynamic and kinematical ways. In kinematic validation, we compare the geometrical characteristics of the wakes. Specifically, we compare the wake structure predicted by DVM-UBC with the experimental results from Strickland [22], with the results obtained with the conformal mapping method proposed in Ref. [24] and with the results obtained by using FLUENT. In dynamic validation, we compare the power coefficient (as a function of TSR) and the dimensionless torque (as a function of azimuth angle). Specifically, we compare the power coefficient obtained with DVM-UBC with the experimental results from Templin [25], the results obtained in UBC experimental tests, and numerical results with FLUENT and traditional DVM. We compare the torque obtained with DVM-UBC with the results obtained in the UBC tests, FLUENT, and traditional DVM.

4.1 Kinematic Validation. Figure 5 shows a comparison of two-dimensional (2D) wake trajectory generated by using DVM-UBC with the experimental results reported by Strickland [22]. The basic specifications of the case include that the turbine has two blades, the turbine's rotating direction is counterclockwise, the blade type is NACA0015, the solidity is 0.3, TSR is 5, and the Reynolds number³ at the design TSR⁴ is 160,000. To conduct a numerical comparison, we analyzed the values of nine particular

³The Reynolds number in the numerical simulation is calculated with respect to incoming flow velocity and blade chord length.

⁴Design TSR refers to the TSR range for which the turbine is designed and under which the power coefficient of the turbine is around its maximum value.

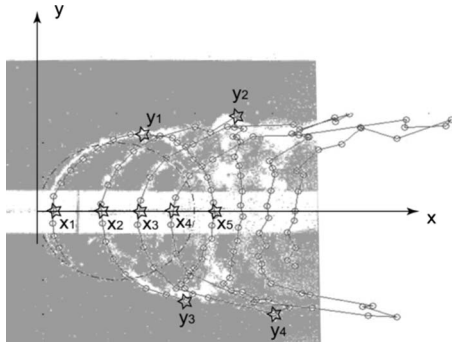


Fig. 5 Wake trajectory generated by using DVM-UBC is superimposed on the wake trajectory in Ref. [22]

Table 1 The relative deviation of the results with DVM-UBC from the experimental results

Position	x_1 (%)	x_2 (%)	x_3 (%)	x_4 (%)	x_5 (%)	y_1 (%)	y_2 (%)	y_3 (%)	y_4 (%)
Relative deviation ^a	4	3	1	4	1	1	1	2	3

^aThe relative deviation here is defined as the ratio of the difference between the numerical value and experimental value to the experimental value. For example, if the experimental value is 0.5 and the numerical value is 0.51, the relative deviation is 2%.

points close to the turbine and found that the free-surface effect in the experimental test may significantly affect the wake trajectory farther downstream. These nine points include the first five cross-axis points (x_1 , x_2 , x_3 , x_4 , and x_5) and the values of the four extreme y points in the first two revolutions (y_1 , y_2 , y_3 and y_4). The comparison results are shown in Table 1. In general, the results generated with DVM-UBC are comparable with the Strickland experimental results. The difference between the experimental results and the results generated with DVM-UBC is within 4% of the experimental value. Therefore, one can say that good agreement was obtained between the DVM-UBC and Strickland [22] results.

Figure 6 shows a comparison of a two-dimensional wake trajectory generated by using DVM-UBC with the results by using a conformal mapping method developed by Delgaire et al. [24]. The basic specifications of this case include that the turbine is a one-blade turbine, the turbine's rotating direction is clockwise, the blade type is NACA0018, the solidity is 0.2, the TSR is 5, and the Reynolds number is 2,000,000.⁵ Again, we compare the values of the first five x -axis points and the value of the four extreme y points in the first two revolutions. The comparison results are shown numerically in Table 2. In general, the results generated with DVM-UBC are comparable with the results obtained with the conformal mapping method. The differences between the results of the two different numerical methods are within 7% of the value generated using the conformal mapping method. Additionally, as the free-surface effect is avoided in both numerical methods, we can also compare the development of the downstream vortices. The geometries of the downstream vortices obtained with both methods are comparable, although the stability of the core vortices seems to be higher in the conformal mapping method. However, it is understood that this conformal mapping method cannot represent the physics of the unsteady flow and the turbine as accurately as DVM-UBC because the conformal mapping method employs the inviscid formulation.

Figure 7 shows a comparison of the growth of the wake generated by DVM-UBC with that generated by FLUENT. The basic

⁵In the conformal mapping method, the Reynolds number is infinite.

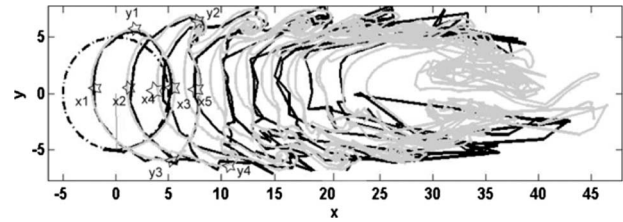
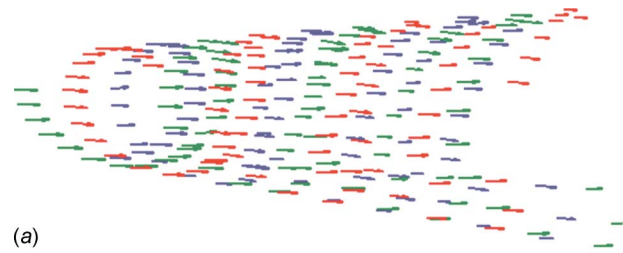


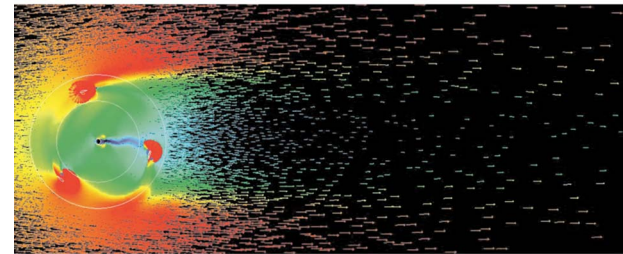
Fig. 6 Comparison of the two-dimensional wake trajectory by using conformal mapping method [24] (gray) and DVM-UBC (black)

Table 2 The relative deviation of the results generated with DVM-UBC from the results generated by using the conformal mapping method

Position	x_1 (%)	x_2 (%)	x_3 (%)	x_4 (%)	x_5 (%)	y_1 (%)	y_2 (%)	y_3 (%)	y_4 (%)
Relative deviation	1	4	5	7	2	1	3	2	2



(a)



(b)

Fig. 7 (a) Turbine wake velocity generated by using DVM-UBC; and (b) turbine wake velocity generated by using FLUENT

specifications of this case include that the turbine is a three-blade turbine, the turbine's rotating direction is clockwise, the blade type is NACA 63₍₄₎-021, the solidity is 0.435, TSR is 2.75, and the Reynolds number is 160,000.⁶ For this case, we could not compare the wake velocity distribution in detail because FLUENT could not provide velocity data at each point. To numerically compare the wake geometry, we defined the wake growth coefficient as

$$C_w = \frac{w_{\text{initial}} - w_{\text{end}}}{l_w} \quad (18)$$

where w_{initial} and w_{end} denote the initial width of the wake (in the y axis direction), and the end width of the wake (where wake velocity is almost the same as the free stream velocity), respectively, and l_w denotes the length (in the x axis direction) between the measure points of w_{initial} and w_{end} . We noted that C_w (DVM-UBC) is equal to 0.325 and C_w (FLUENT) is equal to 0.34, which indicates that the relative deviation of the result obtained with

⁶One might also notice that the turbine simulated using FLUENT has a shaft for the purpose of approximating the turbine in experimental test.

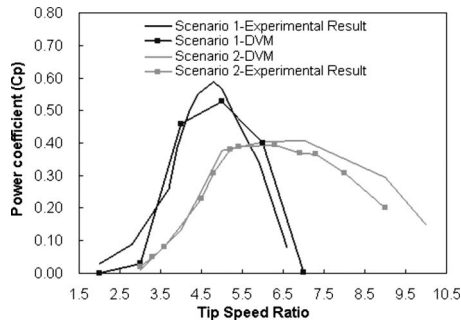


Fig. 8 A comparison of the power coefficient of a stand-alone tidal-current turbine

DVM-UBC from the FLUENT result is less than 6%. That is to say, the results obtained with DVM-UBC are comparable to the results obtained with FLUENT.

4.2 Dynamic Validation. Figure 8 compares the power coefficient, C_p , obtained using DVM-UBC with the results from one of the classical vertical-axis turbine tests reported by Templin [25]. Two scenarios were used for this validation. The basic specifications of Scenario 1 include that the turbine is a three-blade turbine, the blade type is NACA0015, the solidity is 0.25, and the Reynolds number is 360,000. The basic specifications of Scenario 2 include that the turbine is a one-blade turbine, the blade type is NACA0015, the solidity is 0.0833, and the Reynolds number is 360,000. By comparing the maximum power coefficients and corresponding TSR, it can be seen that the relative deviation of the power coefficient obtained with DVM-UBC from the experimental result is about 10% in Scenario 1, and the relative deviation of the power coefficient obtained with DVM-UBC from the experimental results is about 2.5% in Scenario 2. Also, the power coefficient obtained with DVM-UBC is lower than the experimental result when the TSR is lower than the design TSR and is higher when the TSR is higher than the design TSR. This is because the viscous effect varies as the TSR changes.

Figure 9 shows the turbine tested in the UBC towing tank. Because of the time constraints and experiment setup, we were not able to record wake trajectory. Thus, the UBC towing tank test result is only used for dynamic validation not kinematic validation. Figure 10 compares the power coefficient obtained using DVM-UBC with the UBC towing tank test result, and the results generated using other numerical methods (traditional 2D DVM and FLUENT). The basic specifications of this case include that the

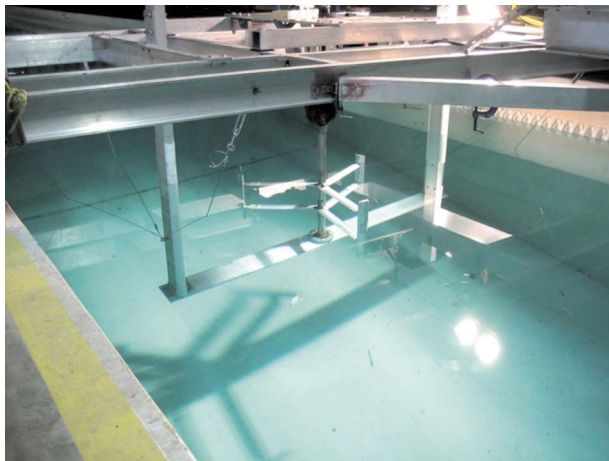


Fig. 9 A snapshot of a turbine being tested in UBC towing tank

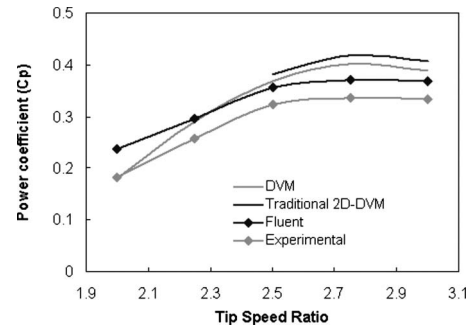
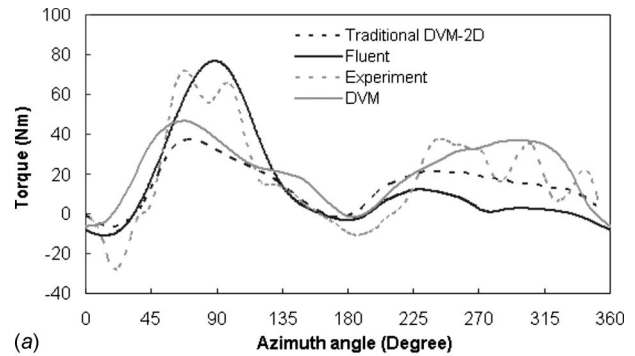
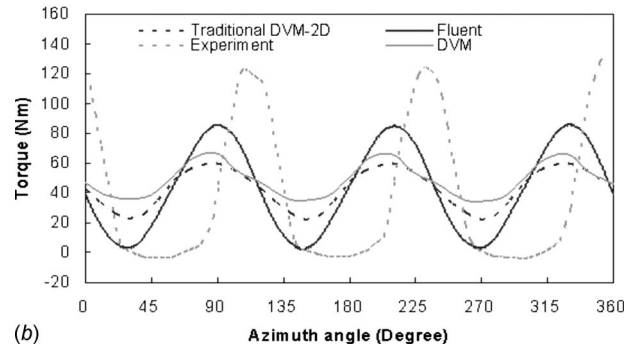


Fig. 10 A comparison of power coefficient of a stand-alone tidal-current turbine by using different methods (DVM-UBC, traditional DVM, FLUENT, and experiment)



(a)



(b)

Fig. 11 The relationship between torque and azimuth angle obtained by using different methods under scenario 1 (a) and scenario 2 (b)

turbine is a three-blade turbine, the blade type is NACA 63₍₄₎-021, the solidity is 0.435, and the Reynolds number is 160,000.⁷ By comparing the maximum power coefficient obtained with these methods, we found that the results have good agreement when the TSR is around 2.75. The relative deviation of the maximum power coefficient obtained with DVM-UBC from the maximum power coefficient obtained using other numerical methods is about 14%. If the FLUENT result is regarded as the exact result, then comparing the relative deviation of the DVM-UBC's result with the FLUENT result (6.7%) and that of the traditional DVM's result with the FLUENT result (13.5%) shows that the results generated by DVM-UBC are much closer to the exact results. In other words, DVM-UBC can predict the turbine performance 50% more accurately than traditional DVM.

Figure 11 compares the torque obtained by using DVM-UBC

⁷The turbine tested in UBC towing tank has two arms and a shaft and the turbine simulated in FLUENT has a shaft.

Table 3 Differences in modeling conditions with different methods

	DVM-UBC	Strickland [22]	Templin [25]	FLUENT	Delgaire et al. [24]	UBC experiment
Steady state	Quasisteady	Unsteady	Unsteady	Unsteady	Steady	Unsteady
Testing area	Unrestricted	Restricted	Unrestricted	Restricted	Unrestricted	Restricted
Free surface	No	Yes	No	No	No	Yes
Turbine position	Fully submerged	Half submerged	Fully submerged	Fully submerged	Fully submerged	Fully submerged
No. of arms	0	1	0	0	0	2
Shaft	No	No	No	Yes	No	Yes
Reynolds number	Quasivariable	Variable	Variable	Variable	Infinite	Variable

with the UBC towing tank test results and with numerical results generated by using other numerical methods (traditional 2D DVM and FLUENT). Two scenarios are validated in this case. The basic specifications of scenario 1 are that the turbine is a one-blade turbine, the blade type is NACA 63₍₄₎-021, the solidity is 0.145, and the Reynolds number is 160,000. The basic specifications of scenario 2 are that the turbine is a three-blade turbine, the blade type is NACA 63₍₄₎-021, the solidity is 0.435, and the Reynolds number is 160,000.

By comparing the maximum torque and the corresponding azimuth angle in Scenario 1, we found that the torque generated by using DVM-UBC is closer to the experimental results than that generated with other numerical methods when the azimuth angle is high (over 200 deg). However, we observed two significant differences: (1) there is a 10–15 deg⁸ phase shift between the numerical and experimental results in Scenario 1 (Fig. 11(a)) and about a 20 deg phase shift in Scenario 2 (Fig. 11(b)); and (2) the maximum torque of the experiment is higher than that generated with DVM-UBC, the minimum torque of the experiment is lower than that generated with the DVM-UBC, and the average torque of the experiment is almost equal to that generated with the DVM-UBC. These two differences are probably caused by the following reasons. (1) The error in experimental set-up: there was no dynamic calibration on the sensor system so that sometimes signal amplification may cause such a phase shift; this issue is quite often observed during ship motion study. (2) The mounted frame effect: the mounted frame is not modeled in any of the numerical methods. (3) The DC motor: the turbine angular velocity controller was unable to maintain a constant angular velocity for a stand-alone turbine during the turbine's rotation, which may be responsible for this phase shift. (4) The towing tank wall effect: we found that the turbine wake is asymmetric, and the width of the towing tank is only 3.7 m. Although there is no blockage effect, the wall effect still amplifies the asymmetry of the wake. The velocity induced by the wake vortices will affect the torque and the corresponding azimuth angle. Thus, the wake asymmetry will affect the torque value and the corresponding azimuth angle.

5 Conclusion and Discussion

This paper mainly describes the formulation and validation process for a new numerical method (i.e., DVM-UBC) for estimating the performance of a stand-alone tidal-current turbine and how this validation process can be used for validating other methods.

⁸The measured torque of one-blade turbine fluctuates significantly. One cannot easily make a judgment about the shift. Comparing the troughs and the peaks between the experimental results and the numerical results, the shifts are slightly different.

We compare its results with that obtained with other methods including traditional DVM, RANS, conformal mapping, and experimental test. In addition to the three-blade torque validation (Fig. 11(b)), the DVM-UBC is consolidated by a systematic validation. Detailed analysis and discussion of these deviations are given in Sec. 5.1.

5.1 Discussion. The results and analysis in this paper show that DVM-UBC can represent the effects of an unsteady wake on the turbine with an acceptable accuracy. The percentage differences between the results generated by DVM-UBC and the reference results in dynamic validation are about two times those in kinematic validation, which may be attributed to the fact that the dynamic results are one order higher than the kinematics results.⁹ Some differences may be caused by the noise and error in the computation and experiment of the unsteady flow and others may be attributed to the differences in the modeling conditions, as summarized in Table 3. For example, shaft effects are unavoidable. The relative deviation of the DVM-UBC's result from FLUENT result is 6.7%; FLUENT simulates the arm while DVM does not. If we use FLUENT to simulate the turbine without the shaft, the deviation is reduced to 1.2%. In the UBC towing tank test, we found that the shaft effects can be significantly reduced by adding a shaft cover. Thus, from an optimal design point of view, we think it is acceptable that DVM-UBC does not simulate the shaft.

Another major reason for the difference between the experimental test and the numerical simulation is the effect of arm connection in the UBC turbine, a significant portion of which can be attributed to the clamping mechanism connecting the blade to the supporting arm. These effects significantly reduce the power coefficient of the turbine because of the parasite drag. In the UBC towing tank test, to test various blades and different configurations, the blade-arm connection is a special mechanism (Fig. 12), which amplifies the drag. Because it will significantly increase the cost to simulate the flexible mechanism in the numerical model, we did not simulate it in DVM-UBC. By using a first order approximation, we found that the arm effect in UBC towing tank test may reduce the power coefficient up to 10%.

5.2 Conclusions. Our study shows that DVM-UBC is a cost-effective accurate method for simulating tidal-current turbines rotating both in clockwise and counterclockwise rotation. We obtained reasonable agreements (in both dynamics and kinematics) for unsteady flow with the UBC experimental results, published experimental results, and the results generated by other numerical methods. DVM-UBC can predict turbine performance almost as

⁹The dynamic result is proportional to the velocity square while the kinematics result is proportional to the velocity.

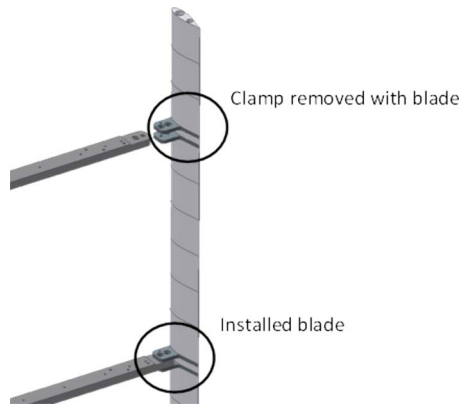


Fig. 12 Blade arm connection

accurately as a commercial RANS, but takes much less time (less than 1% of the time that RANS takes). DVM-UBC is also much less costly than RANS and experimental test.

In addition, DVM-UBC shows a significant improvement over the traditional DVM in predicting the performance of turbines; the results obtained with DVM-UBC are about 50% more accurate than those obtained with the traditional DVM in the cases that we studied. However, the DVM-UBC relies heavily on the availability of hydrodynamic characteristics data. Consequently, errors cannot be avoided when the turbine is not simulated at its design TSR. Arms and shafts are also not simulated in this model, which means that their effects are not included. Therefore, the real turbine efficiency is expected to be less than the numerical prediction.

5.3 Future Work. Based on the experience gained from this study, we identified several relevant issues worthy of further investigation. In addition to the need for quantifying the shaft and arm effects, we must quantify the sea bottom and free-surface effects. The turbine investigated in this paper is assumed to work in an ideal flow where the turbine is far from the water surface and the sea bottom. In the real tidal-current power site, both the water surface and sea bottom are expected to affect the turbine performance based on the change of tidal range. Both analytical and experimental investigations are necessary.

The vortex method developed in this paper only uses a bound vortex to represent the blade element, which cannot represent the near blade phenomenon. Thus, a boundary-element method shall be introduced for further investigation. Evidence shows that a combination of the boundary-element method, the vortex method, and a free-wake structure creates a more accurate tool for marine applications [26]. Different vortex descriptions, such as random vortex method, can be also employed to study the near-field wake. We will also analyze the unsteady torque and its effect on the electric power generator (the voltage and current) under the sea bottom and free-surface effects. A systematic dynamic modeling may be required.

Acknowledgment

The authors would like to thank the following agencies for providing fellowships to Ye Li to conduct this research: UBC, National Science and Engineering Research Council, Society of Naval Architects and Marine Engineers, IEEE, ASME, and ISOPE. The authors would also like to thank Western Economic Diversification and Blue Energy Canada for supporting the experimental test. We would also like to thank Voytek Klaptocz and G. Bill Rawlings for their efforts in designing the prototype and managing the UBC towing tank test as well as the fruitful discussion on the experimental test, and thank Thomas Chabut, Cameron Fraser, John Axerio, Florent Cultot, and Pierre Leplatois for their considerable contributions to the towing tank test.

Appendix

By using the methods for describing and calculating vortices as shown above, we can calculate the performance (force, torque, and power) of a stand-alone tidal-current turbine. For example, after vortex shedding and induced velocity are analyzed, lift can be obtained by using Eq. (7). After obtaining the angle of attack, we can obtain the normal force coefficient and tangential force coefficient with lift and drag coefficient as

$$\begin{pmatrix} C_n \\ C_t \end{pmatrix} = \mathbf{D} \begin{pmatrix} C_D \\ C_L \end{pmatrix} \quad (\text{A1})$$

$$\mathbf{D} = \begin{pmatrix} -\sin \alpha & -\cos \alpha \\ -\cos \alpha & \sin \alpha \end{pmatrix} \quad (\text{A2})$$

where C_n , C_t , and C_D denote normal force coefficient, tangential force coefficient, and drag coefficient, respectively.

We can then use these coefficients to calculate tangential force and normal force according to their definition, as shown in Eqs. (A3)–(A6) and thus to calculate the power output, P , and torque, M , by using Eqs. (A7) and (A8), respectively

$$F_t = \sum_i F_{t,i} \quad (\text{A3})$$

$$F_n = \sum_i F_{n,i} \quad (\text{A4})$$

$$F_{t,i} = \frac{1}{2} C_t \rho b_i c U_R^2 \quad (\text{A5})$$

$$F_{n,i} = \frac{1}{2} C_n \rho b_i c U_R^2 \quad (\text{A6})$$

$$P = M \cdot \omega \quad (\text{A7})$$

$$M = \mathbf{F} \times \mathbf{r} = F_t R \quad (\text{A8})$$

where F_t and F_n denote the tangential force and the normal force, while $F_{t,i}$, $F_{n,i}$, and b_i denote the tangential force, normal force, and blade element length of segment i , respectively.

References

- [1] Li, Y., and Calisal, S. M., 2007, "Preliminary Result of a Discrete Vortex Method for Individual Marine Current Turbine," The 26th ASME International Conference on Offshore Mechanics and Arctic Engineering, Jun. 10–15, San Diego, CA.
- [2] Lang, C., 2003, "Harnessing Tidal Energy Takes New Turn," IEEE Spectrum, 40(9), p. 13.
- [3] Davis, B. V., Swan, D. H., and Kenneth, A., 1981, "Ultra Low-Head Hydroelectric Power Generation Using Ducted Vertical-Axis Water Turbines," National Research Council, Canada, Technical Report No. NEL-002.
- [4] Davis, B. V., Swan, D. H., and Kenneth, A., 1982, "Ultra Low-Head Hydroelectric Power Generation Using Ducted Vertical Axis Water Turbines Location," Canadian National Research Council, Canada, Technical Report No. NEL-022.
- [5] Davis, B. V., Swan, D. H., and Kenneth, A., 1984, "Research on Development of a 50-kw to 100-kw Vertical-Axis Hydro Turbine for a Restricted Flow Installation," Canadian National Research Council, Canada, Technical Report No. NEL-038.
- [6] Batten, W. M. J., Bahaj, A. S., Molland, A. F., and Chaplin, J. R., 2006, "Hydrodynamics of Marine Current Turbines," Renewable Energy, 31(2), pp. 249–256.
- [7] Calcagno, G., Salvatore, F., Greco, L., Moroso, A., and Eriksson, H., 2006, "Experimental and Numerical Investigation of an Innovative Technology for Marine Current Exploitation: The Kobold Turbine," *Proceedings of the International Offshore and Polar Engineering Conference*, pp. 323–330.
- [8] Younsi, R., El-Batanony, I., Tritsch, J. B., Naji, H., and Landjerit, B., 2001, "Dynamic Study of a Wind Turbine Blade With Horizontal Axis," Eur. J. Mech. A/Solids, 20(2), pp. 241–252.
- [9] Nakhla, H., White, D., and Musial, W., 2006, "Structural Dynamics of Small Wind Turbine Blade Under Aerodynamic Loading," 44th AIAA Aerospace Sciences Meeting, Vol. 13, pp. 9431–9442.
- [10] Camporeale, S. M., and Magi, V., 2000, "Streamtube Model for Analysis of Vertical Axis Variable Pitch Turbine for Marine Currents Energy Conversion," Energy Convers. Manage., 41(16), pp. 1811–1827.
- [11] Corio, D. P., Nicolosi, F., De Marco, A., Melone, S., and Montella, F., 2005, "Dynamic Behavior of Novel Vertical Axis Tidal Current Turbine: Numerical

and Experimental Investigations," *Proceedings of the International Offshore and Polar Engineering Conference*, Jun. 19–24, Seoul, South Korea, pp. 469–476.

- [12] Ponta, F. L., and Jacovkis, P. M., 2001, "A Vortex Model for Darrieus Turbine Using Finite Element Techniques," *Renewable Energy*, **24**, pp. 1–18.
- [13] Young, Y. L., Motley, M. R., and Yeung, R. W., (2009), "Three-Dimensional Numerical Modeling of the Transient Fluid-Structural Interaction Response of Tidal Turbines," *ASME J. Offshore Mech. Arct. Eng.*, **131**, p. 011101
- [14] Li, Y., and Çalşal, S. M., (2010), "Numerical Analysis of the Characteristics of a Vertical Axis Water Current Turbine," *Renewable Energy*, **35**, pp. 435–442.
- [15] Wilson, R. E., and Walker, S. N., 1983, "Fixed Wake Theory for Vertical Axis Wind Turbines," *ASME J. Fluids Eng.*, **105**(4), pp. 389–393.
- [16] Jiang, D., Coton, F. N., and Galbraith, McD. R. A., 1991, "Fixed Wake Vortex Model for Vertical Axis Wind Turbines Including Unsteady Aerodynamics," *Wind Eng.*, **15**(6), pp. 348–360.
- [17] Anderson, D. J., 2005, *Fundamentals of Aerodynamics*, 4th ed., McGraw-Hill, New York.
- [18] Streitlien, K., 1995, "Extracting Energy From Unsteady Flow Through Vortex Control," Ph.D. thesis, Massachusetts Institute of Technology (MIT) and Woods Hole Oceanographic Institution (WHOI) Joint Program, MA.
- [19] Bernitsas, M. M., Raghavan, K., Ben-Simon, Y., and Garcia, E., 2006, "VI-VACE (Vortex Induced Vibration Aquatic Clean Energy): A New Concept in Generation of Clean and Renewable Energy From Fluid Flow," *Proceedings of 25th International Conference on Offshore Mechanics and Arctic Engineering, OMAE*.
- [20] Graham, J. M. R., 1977, "Vortex Shedding From Sharp Edges," Imperial College Aero. Report No. 77-06.
- [21] Kudo, K., 1981, "Hydrodynamics Forces of the Oscillating Flat Plate," *Proceedings of the Third International Conference on Naval Hydrodynamics*.
- [22] Strickland, J. H., 1975, "The Darrieus Turbine: a Performance Prediction Model Using Multiple Streamtubes," Sandia National Laboratory, Albuquerque, NM, Report No. 74-0431.
- [23] Li, Y., 2008, "A Procedure of Predicting the Power Output From a Tidal-Current Turbine Farm," Ph.D. thesis, the University of British Columbia.
- [24] Deglaire, P., Agren, O., Bernhoff, H., and Leijon, M., 2008, "Conformal Mapping and Efficient Boundary Element Method Without Boundary Elements for Fast Vortex Particle Simulations," *Eur. J. Mech. B/Fluids*, **27**(2), pp. 150–76.
- [25] Templin, R., 1974, "Aerodynamic Performance Theory for the NRC Vertical-Axis Wind Turbine," National Aeronautical Establishment Lab, National Research Council, Canada, Technical Report No. LTR-LA-160.
- [26] Yeung, R., 2002, "Fluid Dynamics of Finned Bodies—From VIV to FPSO," 12th International Offshore and Polar Engineering Conference, Vol. 2, Kitakyushu, Japan, pp. 1–11.